Enhancing Dispersibility of Paramylon Nanofiber Suspensions through Water-Jet Defibrillation Treatment

Takefumi NARITA[1,*], Juna KOIZUMI[2], Kasumi WADA[2], Ryo NAKADA[2],
Ikuhiro TANIDA[2], Satoshi OSAWA[2]

Abstract

In this study, paramylon nanofiber suspensions (PNFSs) with different dispersibility were developed by adjusting the pretreatment conditions, including pretreatment time and concentration of paramylon granules. The rheological, tribological, and chemical properties of the resulting PNFSs were evaluated. Two types of paramylon nanofiber (PNF) were prepared through water-jet (WJ) defibrillation: PNF-MP1, which underwent a short pretreatment time and low concentration and PNF-MP2, which underwent a long pretreatment time and high concentration. The defibrillation treatment partially converted PNF-MP1 to fibers, with some granules remaining. In contrast, PNF-MP2 obtained excellent nanofiber formation owing to the accelerated defibrillation effect. The rheological evaluation revealed that PNF-MP2 exhibited the highest dispersibility and the reversibility of viscosity recovery. Friction property evaluation showed that PNF-MP2 displayed excellent lubrication effects. Wide angle X-ray diffraction (WAXD) analysis showed that the defibrillation treatment impaired the microcrystallization and crystal regularity of PNF. X-ray photoelectron spectroscopy (XPS) surface elemental analysis showed that the defibrillation treatment exposed hydroxyl groups on the PNF surface, enhancing its hydrophilicity.

Keywords：Paramylon, Nanofiber, Defibrillation, Water-jet, Dispersibility

Received July 11, 2023; accepted July 29, 2023

1) Industrial Process Technology Group, Tokyo Metropolitan Industrial Technology Research Institute, 2-4-10, Aomi, Koto-ku, Tokyo 135-0064, Japan

2) Genome Biotechnology Laboratory, Kanazawa Institute of Technology, 3-1, Yatsukaho, Hakusan, Ishikawa, 921-8501, Japan

*Corresponding author: Takefumi Narita, E-mail: narita.takefumi@iri-tokyo.jp

1. Introduction

The effective utilization of biomass is becoming increasingly important toward realizing carbon neutrality[1]. Biomass, including cellulose, chitosan, and chitin, has excellent environmental and biocompatible properties and is being explored for various applications in a wide range of fields, including medicine[2], food[3], and paints[4]. In recent years, nanofibers derived from biomass resources have emerged as a novel avenue to develop new applications[5].

Cellulose, the most abundant biomass on earth, is derived from plants and wood and can be processed into nanofibers through physical and chemical treatments and mechanical crushing and shearing. These nanofibers are used as reinforcing fibers[6] for polymers and other materials[7]. Chitin and deacetylated chitosan extracted from crustaceans, such as crabs and shrimps, are also being developed as food additives by improving their water dispersibility through nanofiber formation[8].

Paramylon, a β-1, 3-glucan produced by the microalga Euglena, shares a similar structure with cellulose[9]. The crystal structure of paramylon comprises elliptical granules of β-1, 3-glucan with a diameter of 1–4 μm, forming a triple-helical crystal structure, and the granules are porous[10]. Paramylon possesses the advantage of consistent properties and shapes across different strains of Euglena, facilitating the production of raw materials with identical properties[11]. Previous studies have reported utilizing paramylon for plastic moldings[12] and nanofibers[13]. However, the conversion of paramylon into nanofibers has problems in the manufacturing process, such as the use of strong alkaline solutions containing considerable amounts of sodium hydroxide, as well as the inevitable inclusion of sodium chloride and other substances during neutralization. Therefore, it is desirable to minimize the use of organic solvents during nanofiber fabrication.

Against this background, we previously reported a technique for preparing nanofibers using only water and raw materials through WJ treatment. This approach showcased excellent functionalities of nanofibers, such as larger specific surface area and higher biocompatibility compared to cast films obtained with dilute acid when nanofibers are converted into a film[14]. However, paramylon granules exhibit oil and water absorption and have affinity for both hydrophilic and lipophilic materials[15]. Therefore, focusing on the unique structure of paramylon and enhancing the water dispersibility of paramylon nanofibers through this fabrication technology using WJ is expected to be developed as additives in water-based paints and other applications, reducing volatile organic compounds.

In this study, we attempted to develop highly dispersible PNFSs by modifying the pretreatment conditions of paramylon granules. The rheological, tribological, and chemical properties of PNFSs with different dispersibility were evaluated, and detailed findings were reported.

2. Material and Methods

2.1. Materials. Paramylon powder from *Euglena gracilis* (*E.gracilis*) (IRIAL Corporation), sodium dodecyl sulfate (SDS) (FUJIFILM Wako Pure Chemical Corporation), n-hexane (FUJIFILM Wako Pure Chemical Corporation) were purchased.

2.2 Isolation of paramylon. In a 50 mL Falcon tube, 3 g of dry powder of Paramylon was dispersed in 20 mL of reverse osmosis (RO) water. To crush the cell membranes of Paramylon, the Paramylon powder were sonicated in ice-cold water for 30 min using an ultrasonic homogenizer (LUH150; Yamato Scientific Co., Ltd.), followed by centrifugation at 6,000 rpm for 5 min using a centrifuge (Himac CF 15R; Hitachi-Koki

Corporation) to remove the supernatant fluid. The Falcon tube was then filled with 20 mL of RO water and 10 mL of n-hexane, sonicated for 5 min, and centrifuged again at 6,000 rpm for 5 min. This purification process was repeated six times to increase the purity of the precipitate. To remove the oil component, 20 mL of 80 vol% acetone solution was dispersed in this Falcon tube, sonicated for 5 min, centrifuged again at 6,000 rpm for 5 min, and the supernatant liquid was removed. This process was also repeated six times. The precipitate was dispersed in 20 mL of RO water and filtered through a filter (53 μm aperture). The filtered precipitate was heat-dried at 80 °C, and the resulting granules were powdered using an agate mortar. To remove the supernatant liquid, the powder was added to 20 mL of RO water and sonicated in ice-cold water for 30 min using an ultrasonic homogenizer, followed by centrifugation at 6,000 rpm for 5 min using a centrifuge. To remove other proteins, 20 mL of 1 wt% SDS solution was added and washed in a water bath at 90 °C for 10 min. The solution was centrifuged at 6,000 rpm for 5 min to remove the supernatant, and this procedure was repeated three times. Then, 20 mL of RO water was added to the precipitate to remove any remaining SDS. The solution was centrifuged at 6,000 rpm for 5 min to remove the supernatant. This procedure was performed until the foam in this solution was eliminated. The remaining precipitate was heat-dried, and the resulting granules were powdered in an agate mortar, which was used in this study as paramylon granules.

2.3 Preparation of PNFSs. The paramylon granules obtained in section 2.2 were pretreated before defibrillation. Two different manufacturing processes (MP) were employed as pretreatments for fibers to achieve nanofiber refinement, as shown in Fig 1. Nanofiberization was performed using WJ treatment on paramylon dispersion with different defibrillation pretreatment methods. PNFSs were obtained using a tabletop wet atomizer (HJP-25001SE; Sugino Machine Co., Ltd.), pressurized at 200 ± 20 MPa, and ejected through a fine nozzle. The dispersion impacted ceramic balls multiple times to promote defibrillation. Specifically, the PNFSs were obtained by subjecting the dispersion to five impacts with ceramic balls. The PNFSs obtained using MP1 are denoted as PNF-MP1, while those obtained using MP2 are referred to as PNF-MP2. For subsequent measurements, PNFSs adjusted to 5 wt% were used (PNF-MP1 was adjusted to 5 wt% by collecting the supernatant solution.).

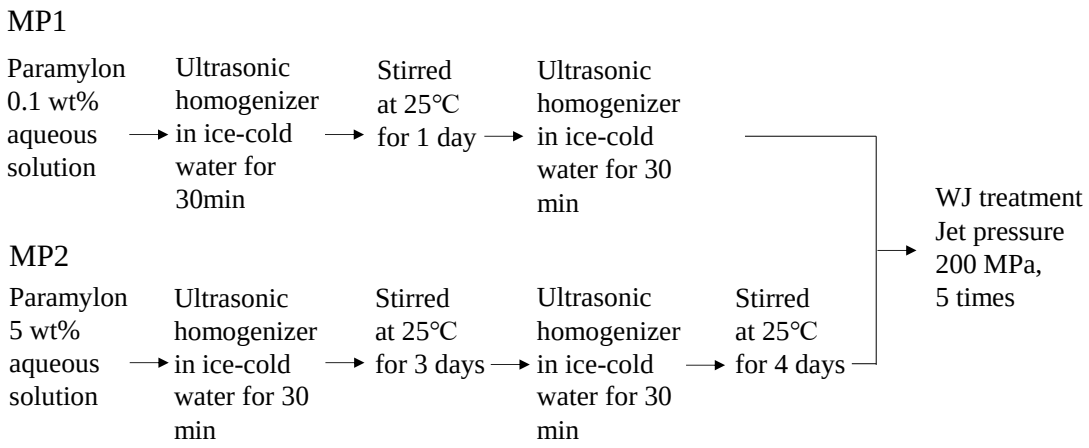

Fig 1. MP of PNFSs by Water-Jet defibrillation treatment.

2.4 Morphological analysis through scanning electron microscope. The samples were observed using a scanning electron microscope (SEM, SEM EDX MP N; High-Technologies Corporation). Before observation, the samples were fixed to a specimen stand using carbon tape, and then gold/palladium alloy was deposited using an ion sputtering apparatus (E-1010; Hitachi High-Technologies Corporation).

2.5 Rheological properties of PNFSs. The rheological properties of the PNFSs were measured using a rheometer (MCR302; Anton Paar). The sensor geometry was selected according to the viscosity of the sample, and a cone-plate sensor (diameter = 35 or 50 mm, angle = 1° or 2°) was used. The measurement temperature was 25 °C. For steady-state flow viscosity measurements, the shear stress was determined at a shear rate of 0.01 to 1,000 s^{-1}. The viscosity recovery was examined for the structural recovery measurement when the shear rate was varied in the order of 0.1, 500, and 0.1 s^{-1}.

2.6 Friction properties of PNFSs. The frictional properties of the PNFSs were measured using the ball-on-3-pin tribocell setup supplied with the rheometer. The ball was made of SUJ2 with a diameter of 12.7 mm and a surface roughness of Ra 0.1 mm. The pin was a SUJ2 cylinder with a diameter of 6.0 mm and a thickness of 6.0 mm, and its surface roughness was Ra 0.1 mm, measured perpendicular to the sliding direction. The measurement temperature was 25 °C. The sliding velocity of friction was measured at a load of 10 N (P_{mean} = 0.85 GPa) and a sliding velocity of 0.000001 to 0.1 m/s.

2.7 Crystal structure through WAXD. WAXD analysis was performed on an X-ray diffractometer (Ultima IV; Rigaku Corporation) with a monochromatic CuKα line generated at 30 kV and 20 mA. The measurement conditions included a scanning range of 2θ = 4°–40°, a 2θ step of 0.02°, and a scan speed of 2°/min using a divergence slit of 1°, scattering slit of 1°, and receiving slit of 0.15 mm.

2.8 Surface analysis through XPS. X-ray Photoelectron Spectroscopy (XPS) analysis was performed with an X-ray photoelectron spectrometer (ESCA-3400; Shimadzu Corporation). The measurement conditions involved a vacuum of < 10^{-4} Pa, a current of 10 mA, and irradiation with MgKα rays generated at 10 kV.

3. Results and Discussion

3.1 Observation of shape of PNFSs. Fig. 2 shows the results of defibrillation of paramylon granules. PNF-MP1 showed granule shape before defibrillation (Fig.2(A)), but many granules remained after WJ treatment (Fig.2 (B)). PNF-MP2 showed expansion of granules by increasing the treatment time before defibrillation (Fig.2 (C)). After defibrillation with WJ treatment, the enlarged granules were observed to reduce in size, which suggests the possibility of fiber formation (Fig.2(D)). To confirm the fiber morphology, morphological observations after dilution of WJ-treated PNF-MP2 (Fig.2 (D)) to 0.1 wt% with RO water are shown in Fig. 3. As a result, the fiber morphology of paramylon was confirmed in Fig. 3(A). In Fig.3(B), fiber diameters of several hundred nm were observed under high magnification (×11k), indicating that

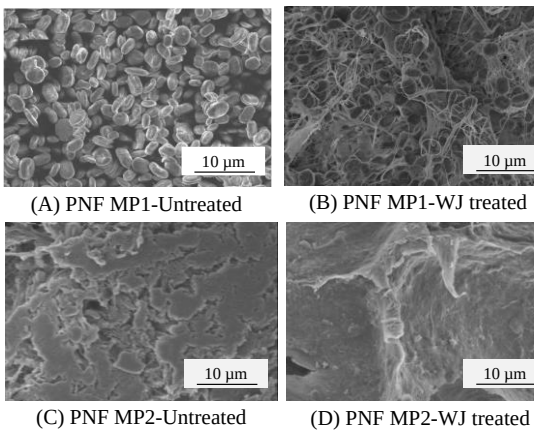

(A) PNF MP1-Untreated (B) PNF MP1-WJ treated

(C) PNF MP2-Untreated (D) PNF MP2-WJ treated

Fig 2. SEM photographs of PNFSs.

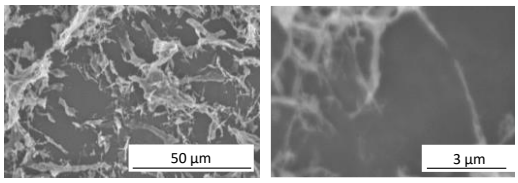

(A) PNF-MP2 (B) PNF-MP2

Fig 3. SEM photographs of diluting WJ-treated PNF-MP2 to 0.1 wt% with RO water.

PNF-MP2 is a nanofiber. It is suggested that the longer pretreatment time allowed for higher penetration into the granule interior, and the higher concentration allowed for a larger surface area of PNF, thereby promoting the effect of the defibrillation treatment to the interior of the granules.

3.2 Rheological properties of PNFSs. Steady flow viscosity measurements of PNFSs are shown in Fig. 4. Paramylon granules showed a significant decrease in shear stress at a shear rate of around 10 s^{-1}, followed by an increase in shear stress again, but at the lowest value. PNF-MP1 showed shoulder peaks of shear stress similar to that of paramylon granules at shear rates of 5 s^{-1} and around 100 s^{-1}, followed by an increase in shear stress again. This indicates that the granules and agglomerates of nanofibers are broken down as the shear rate increases. Therefore, the low effect of the defibrillation process means that more granule-like solids and agglomerated components were included.

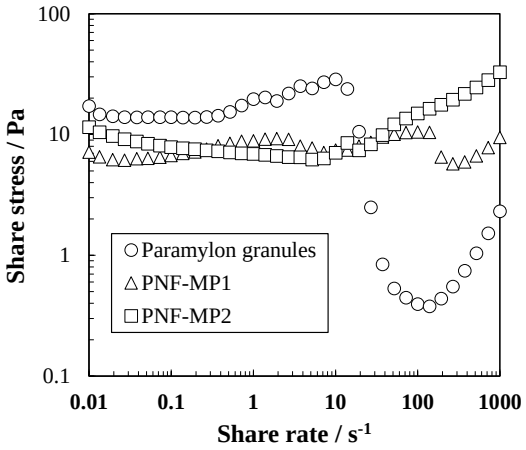

Fig 4. Shear stress curves as a function of shear rate for PNFSs.

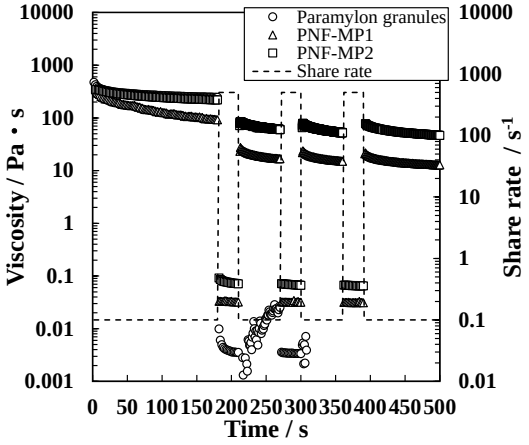

Fig 5. 3-step shear rate curve (0.1 s^{-1} →500 s^{-1} → 0.1 s^{-1}) of PNFSs.

On the other hand, PNF-MP2 showed a monotonous increase in shear stress, and no shoulder peak of shear stress was observed. This means that there were no granule-like solids due to the most advanced defibrillation process with the highest pretreatment effect. Therefore, PNF-MP2 was found to have the highest dispersibility.

The thixotropy (viscosity recovery) of the samples was investigated when the shear rate was changed stepwise with respect to the measurement time. Fig.5 shows the change over time in viscosity when the measurement was repeated three times, with one cycle consisting of a measurement at a low shear rate (0.1 s^{-1}) followed by a measurement at a high shear rate (500 s^{-1}) and then again at a low shear rate (0.1 s^{-1}). The results show that the viscosity of paramylon granules decreased significantly at high shear, and there was almost no viscosity recovery when the low shear rate was returned again. In the second cycle, the measurement was interrupted because it fell below the lower torque limit value. A subsequent comparison of PNF-MP1 and MP2 showed that both samples exhibited structural breakdown after one cycle of high shear rate, but viscosity was higher for PNF-MP2. The same degree of viscosity recovery was also observed after the second cycle, indicating that the collapse and recovery of the inter-fiber

structure continued after structural failure. This suggests that the high dispersion of nanofibers due to the pretreatment effect of PNF-MP2 resulted in a higher entanglement effect between nanofibers and stabilized structural recovery.

3.3 Friction Characteristics of PNFSs. In the previous section 3.2, rheological evaluation showed that PNF-MP2 has high dispersibility in aqueous solution due to the elimination of granules by WJ treatment. PNF-MP1 exhibits lower uniformity due to the mixture of granules and partial fibers in the aqueous solution, while PNF-MP2 indicates that nanofibers are uniformly dispersed in the aqueous solution. Therefore, NF aqueous solutions with different dispersibility may exhibit different frictional properties. To investigate the frictional properties of nanofibers with different dispersibility in an aqueous solution, the coefficient of friction was evaluated. Fig. 6 shows the results of the coefficient of friction for PNFSs on the SUJ2 contactor. Paramylon granules showed the highest coefficient of friction and no lubrication effect. Comparing PNF-MP1 and MP2, PNF-MP2 showed the lowest friction coefficient and the highest lubrication effect. In particular, the coefficient of friction is significantly reduced in the boundary lubrication zone with a sliding velocity of 10^{-4} m/s or less. These results indicate that the frictional properties in the boundary lubrication zone differ greatly due to different dispersibility. In general, it is known that in polymer friction modifiers (PFMs), the PFMs are adsorbed on the oxide film surface of the contactor, forming an adsorbed molecular film that has a high friction reducing effect[16]. This suggests that the friction reduction effect is enhanced by the adsorption on the contactor surface in aqueous environments due to changes in the crystal structure of paramylon and the chemical properties on the PNF surface caused by the PNF-MP2 defibrillation treatment effect.

3.4 Crystal Structure by WAXD analysis. WAXD analysis was performed to clarify change in crystal structure due to the defibrillation treatment. Fig. 7 shows the WAXD of PNF-MP2 with the highest dispersion and paramylon granule. The major reflections 2θ = 7.0 °, 16.7 °, 19.4 °, 20.7 ° and 24.1 ° are due to (100), (101), (111), (201) and (121) planes, respectively[17]. The diffractions become broadened by the defibrillation treatment. Assuming the mosaic model, we estimated the crystallite size (D) normal to the (100) plane using Scherrer's equation (1).

$$D=(K\lambda)/(\beta\cos\theta) \quad \cdots\cdots \quad (1)$$

where K=shape factor (0.9), λ=wavelength of X-rays targeted to Cu (CuKα; 1.54Å), β=width at half

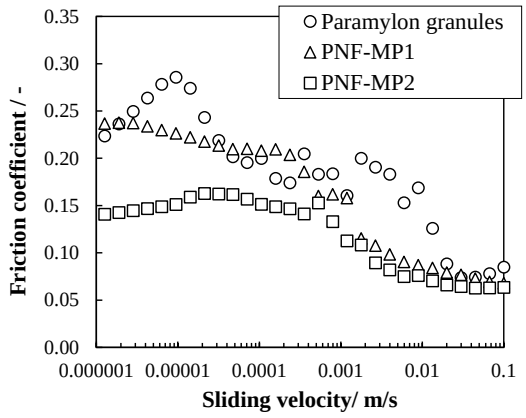

Fig 6. Frictional properties of PNFSs.

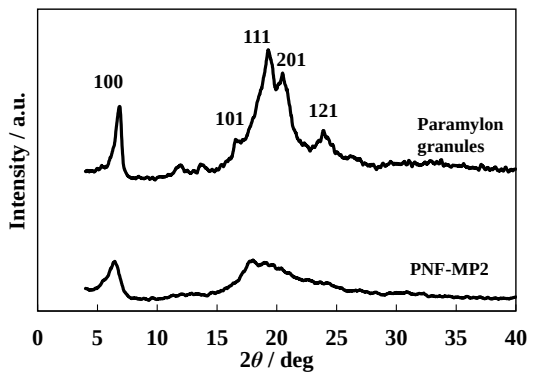

Fig 7. WAXD patterns of Paramylon granules and PNF-MP2.

maximum, and θ=Bragg angle.

The D_{100} for paramylon granules and PNF-MP2 were approximately 176 Å and 68 Å, respectively. This indicates that the crystallite size in the fibers radial direction decreased due to the disassembly of fibers perpendicular to the C-axis (fiber length direction). The WAXD profile of PNF-MP2 is significantly broader compared to that of paramylon granules, suggesting that the crystalline regularity was also lost as the defibrillation process progressed, leading to amorphization.

3.5 Surface Analysis by XPS. In the previous section 3.4, it was found that the crystalline regularity is lost and amorphized by the defibrillation treatment. In order to clarify the difference in the surface properties of PNF due to the defibrillation treatment, Fig. 8 shows a narrow scan of the C1s of paramylon granules, PNF-MP2. The peak area ratios of the binding modes of the C 1s spectra from the results of Fig. 8 are shown in Table 1. The results show that the peak area ratio of the hydroxy group (OH) of PNF increased compared to that of the paramylon granules. This suggests that the pretreatment effect of MP2 penetrates into the interior of the granules, which promotes nanofiber formation during the WJ defibrillation process and further exposes the hydroxy groups on the PNF surface to the material surface when microcrystallization and crystal regularity are impaired, thereby improving the hydrophilicity of the material. Therefore, it is thought that the material became highly dispersible without solid components such as granules, resulting in higher water dispersibility. The above results indicate that the rheological properties of the PNF material indicate that the water dispersibility is increased, and the lubricating effect is also increased due to the higher polarity.

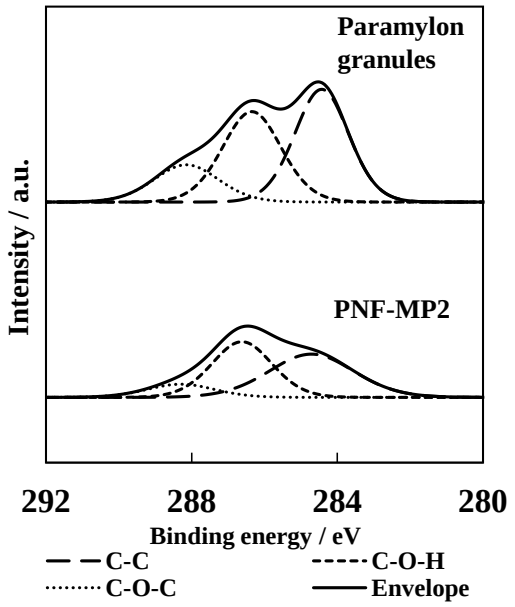

Fig 8. Narrow scan spectrum of the C1s region of Paramylon granules and PNF-MP2.

Table 1. Area ratio of binding mode of C1s spectrum

Binding mode	Paramylon granules	PNF-MP2
C-C	44.1	46.5
C-O-H	38.5	42.3
C-O-C	17.4	11.2

4. Conclusion

In this study, PNFSs with different dispersibility were developed by adjusting the pretreatment conditions, including pretreatment time and concentration. Through defibrillation treatment, PNF-1 exhibited limited fiber formation, with granules still present, while PNF-MP2 demonstrated an accelerated defibrillation effect, resulting in the formation of well-dispersed nanofibers. The rheological evaluation showed that PNF-MP2 exhibited the highest dispersibility and the reversibility of viscosity recovery. among the samples. The friction property evaluation showed that PNF-MP2 has a high lubrication effect. WAXD analysis showed that the defibrillation treatment substantially affected the microcrystallization and

crystal regularity of PNF, while XPS surface elemental analysis revealed an increased exposure of hydroxyl groups on the PNF surface, resulting in improved hydrophilicity. The defibrillation treatment effect enhanced the hydrophilicity of PNF was improved by exposing hydroxyl groups on its surface. These findings indicate that paramylon nanofibers, produced through the WJ fiber treatment without organic solvents, have excellent water dispersibility. Consequently, they hold great potential for applications in water-based paints and related industries.

References

1) A. Isogai, J. Fiber Sci. Technol., **2020**, *76*, 310-326

2) D. Li, Y. Wang, W. Huang, H. Gong, Frontiers in Materials, **2023**, *10*, 1058050.

3) F. Shahidi, J. K. V. Arachchi, Y. Jeon., Trends Food Sci Tech., **1999**, *10*, 37-51

4)L. Wang, P.V. Kelly, N.Ozveren, X. Zhang, M.Ko rey, C.Chen, K.Li, S.Bhandari, H.Tekinalp, X.Zhao, J.Wang, M.Ö.Seydibeyoğlu, E.A. Seydibeyoglu, W. M. Gramlich, M. Tajvidi, E. Webb, S.Ozcan, D. J. Gardner, Matter., **2023**, *6*, 344-372

5) J. Pennells, V. Mellor, D. J. Martin, ACS Sustain. Chem. Eng., **2022,** *10*, 3623-3632

6) S. Keita., M. Yoshihito, T. Yoshinobu, J. Fiber Sci. Technol., ***2020,*** *76*, 23-31

7) M. Fazeli, R. A. Simao, Plasma Process Polym., **2019,** *16*, e1800167

8) H. Tanaka, M. Egusa, Y. Takemura, Y. Iwata, T. Nagae, S. Ifuku, H. Kaminaka, Nippon Shokuhin Kagaku Kogaku Kaishi, **2016**, *63*, 18-24.

9) Y. Kawahara, Carbohydr. Polym., **2014**, *112*, 73-76.

10) K. Kobayashi, S. Kimura, E. Togawa, M. Wada, S. Kuga, Carbohydr. Polym., **2010,** *80*, 491-497

11)M. Shibakami, J of Oleo Science, **2023**, *2*, 87-93

12) M. Shibakami, G. Tsubouchi, M. Hayashi, Carbohydr. Polym., **2014**, *105*, 90-96.

13) M. Shibakami, G. Tsubouchi, M. Nakamura, M. Hayashi, Carbohydr. Polym., **2013,** *93*, 499-505.

14) Y. Yoshikawa, T. Narita, S. Osawa, Kobunshi Ronbunsyu, **2013**, *70*, 668-673

15) K. Suzuki, R. Nakano, H. Yamaguchi, A. Maruta, Y. Nakano., J.Soc.Powder Technol. Japan, **2013**, *50*, 728-732

16) Y. Deslandes, R. H. Marchessault, A. Sarko, Macromolecules, **1980**, *13*, 1466-1471

17) K. Nakamura, M. Muraki, J. Jpn. Soc. Tribol., **2007**, *52*, 687-695